Three-dimensional crystals of CaATPase from sarcoplasmic reticulum

Symmetry and molecular packing

David L. Stokes*‡ and N. Michael Green*

*National Institute for Medical Research, London NW7 1AA; and ‡Laboratory of Molecular Biology, Cambrige CB2 2QH, United Kingdom

ABSTRACT Structural studies of CaATPase from sarcoplasmic reticulum have so far been restricted to low resolution due to the poor order of two-dimensional crystal forms. However, we report that three-dimensional microcrystals of detergent-solubilized CaATPase diffract to 7.2 Å in x-ray powder patterns and may therefore provide an opportunity to study CaATPase structure at higher resolutions. In the present study, we have characterized the symmetry and molecular packing of negatively stained crystals by electron microscopy (em). By altering the detergent-to-lipid ratio, different sized crystals were produced, which adhere to an em grid in different orientations. Thus, we obtained micrographs of three different projections and from these determined unit cell dimensions to be 151 × 51 × 158 Å and the three-dimensional space group to be C2 with an angle β very close to 90°; x-ray powder patterns of hydrated, unstained crystals yielded dimensions of 166 × 58 × 164 Å. Micrographs from each of two principal projections were averaged to produce two-dimensional density maps. Based on these maps and on the previously determined low-resolution structure of CaATPase, a packing diagram for these three-dimensional crystals is presented and major intermolecular contacts are proposed.

INTRODUCTION

CaATPase is a transmembrane protein that uses ATP to transport Ca^{++} from the sarcoplasm into the lumen of sarcoplasmic reticulum (SR), thus participating in the control of muscle contraction. An enormous amount of work has addressed, among other things, the mechanism of Ca^{++} pumping, the sites of ligand binding, and the amino acid sequence. Thus, the reaction cycle has been thoroughly characterized under a variety of different conditions (Inesi, 1985) and regions of the amino acid sequence are currently being associated with specific steps in this cycle, e.g., ATP hydrolysis and Ca^{++} transport (Maruyama and MacLennan, 1988; Clarke et al., 1989). Despite these results, the physical coupling between these two fundamental steps remains obscure and is likely to be revealed only by combining available information with the high-resolution three-dimensional structure of CaATPase.

Structural studies of CaATPase, like those of many membrane proteins, have so far provided only low-resolution structures. In particular, native SR membranes, with a disordered arrangement of CaATPase, have been studied by x-ray diffraction, resulting in a cylindrically averaged profile for the molecule (Herbette et al., 1985). In addition, two kinds of two-dimensional crystals have been discovered, which are distinguished by conditions of crystallization and molecular packing. The different packing is thought to reflect different enzymatic states of CaATPase molecules within the two types of crystals; therefore, they are called E_1 and E_2 crystals after the two states of the reaction cycle (Martonosi et al., 1987). The E_2 crystals are somewhat larger and better ordered, and electron microscopy has therefore resulted in three-dimensional reconstructions (Castellani et al., 1985; Taylor et al., 1986 *a* and *b*). However, due to the limited diffraction from these crystals (25 Å resolution), the reconstructions only define the surface contours of the molecule, its disposition in the membrane, and the intermolecular contacts, and do not suggest a structural basis for the reaction mechanism.

Growth of three-dimensional crystals represents a key step in obtaining high-resolution structures of membrane proteins; therefore, the discovery of three-dimensional microcrystals of CaATPase (Dux et al., 1987) is a significant advance. General experience indicates that there are two types of three-dimensional crystals of membrane proteins (Michel, 1983). On the one hand, "type I" crystals are composed of stacks of two-dimensional crystals. The individual layers comprise planar membranes, which incorporate intramembranous domains of the protein, and stacking is mediated by hydrophilic interactions between extramembranous domains. Very few crystals of type I exist, about four according to Kühlbrandt (1988*b*); they are all quite small and the two best studied examples contain serious stacking defects (Henderson and Shotton, 1980; Kühlbrandt, 1988*a*). On the other hand, "type II" crystals are characterized by a

0006-3495/90/01/1/14 $2.00

more isotropic arrangement of fully solubilized molecules, similar to crystals of many soluble proteins. All intermolecular contacts are thought to occur between hydrophilic surfaces, thereby providing crystallization conditions that are more easily optimized. Crystals both of bacterial photosynthetic reaction center (Deisenhofer et al., 1985) and of porin (Garavito et al., 1983) are of this type and have been studied at atomic resolution by x-ray crystallographic analysis.

The three-dimensional microcrystals of CaATPase, according to a recent electron microscopic study (Taylor et al., 1988), are stacks of two-dimensional crystals, implying that they belong to type I. The crystals used in this study, however, were poorly ordered and we report here on conditions for growing larger, better ordered microcrystals and on their analysis both by x-ray diffraction and by electron microscopy. The resulting x-ray powder patterns show diffraction to 7 Å resolution and contain clear evidence for ordered stacking; thus, this may be the first example of a well-ordered, type I crystal. In addition, electron micrographs of negatively stained crystals indicate that the three-dimensional space group is C2 and provide density maps of two orthogonal projections, based on which we propose a model for packing CaATPase in the crystals.

METHODS

Preparation and crystallization of CaATPase

Four previously described preparations of CaATPase from the white muscle in the back and hind legs of rabbit were used to study crystallization. The first followed the method of Martonosi (1968) and involved a final separation of SR from other components on a sucrose gradient (referred to as SR1). The second (Lüdi and Hasselbach, 1985) involved solubilizing SR1 with cholate and then centrifuging this solution through a discontinuous sucrose gradient (SR2). The third (MacLennan, 1970) involved solubilization with deoxycholate and fractionation with ammonium acetate as the final purification step (SR3).

The last preparation (SR4) relied on a reactive red affinity column (Coll and Murphy, 1984). Because the conditions used were somewhat different from those reported by Coll and Murphy and because this preparation produced the best crystals, this procedure will be described in more detail. Before loading this column, 125 mg of SR1 was solubilized in 25 ml of 100 mg/ml $C_{12}E_8$ (octaethylene glycol dodecylether), 8 mM $CaCl_2$, 1 mM $MgCl_2$, 50 mM Pipes (pH 7), 20% glycerol, 1 mM DTT. Insoluble material was removed by centrifugation at 150,000 *g* for 15 min, and the supernatant was loaded at 20 ml/h onto a freshly packed column (1 × 6.25 cm, type 3000CL from Sigma Chemical Co., St. Louis, MO). For efficient elution, it was essential to saturate the column with CaATPase; therefore, the level of saturation was monitored by measuring ATPase activity in fractions coming off the column during loading. After loading all 25 ml of starting material, this eluted activity was generally about half that of the starting material, which proved to be sufficient saturation. The column was then washed with 1 column volume of wash buffer (1 mg/ml $C_{12}E_8$, 1 mM $CaCl_2$, 1 mM $MgCl_2$, 20 mM EPPS pH 8, 20% glycerol, 1 mM DTT) and purified CaATPase was eluted at 12–15 ml/h with 2 mM ADP in this same buffer. Peak protein concentration was usually 1.5 mg/ml and after combining peak fractions, the yield was typically 20 mg at 1 mg/ml.

A DEAE ion exchange column was used to partially delipidate SR1 and SR3 and to concentrate SR4 (Green, 1975). Preparations of SR1 and SR3 were first solubilized at 10 mg/ml in 60 mg/ml $C_{12}E_8$, 20% glycerol, 20 mM EPPS (pH 8), 6 mM $CaCl_2$, 1 mM DTT, and centrifuged at 150,000 *g* for 15 min to remove insoluble material. In each case, the solution was loaded onto a freshly packed DEAE ion exchange column (1.5 × 6 cm) at 30 ml/h. After washing with 0.5–1 column volume of wash buffer, the protein was eluted with 300 mM NaCl in wash buffer at 15 ml/h. Peak fractions were 6–12 mg/ml and the concentrations of pooled fractions were 4–8 mg/ml. All columns were run at 4°C.

All preparations of CaATPase crystallized in a solution of 100 mM KCl, 3 mM $MgCl_2$, 20% glycerol, 20 mM MES (pH 6), 5 mM DTT, 1 mM NaN_3, 1–10 mM $CaCl_2$, and a range of $C_{12}E_8$/lipid/protein molar ratios from 25:25:1 to 200:100:1 (see Results). Whereas detergent and lipid were added directly to protein solutions, pH and salt concentrations were adjusted either by dialysis or dilution into the appropriate buffer. Lipid was prepared as a stock solution in chloroform and then dried into a thin film, resuspended in buffer, and sonicated for ~5 min with a probe sonicator. Crystallization tubes were purged with N_2 and stored at 4°C. After a few days or a week, microcrystals formed a white sediment in the bottom of the tubes.

Electron microscopy

Crystals were negatively stained for electron microscopy by pipetting a few microliters of crystal sediment onto a glow-discharged, carbon-coated em grid. After 15–30 s, this solution was removed and replaced by three successive drops of 1% uranyl acetate over a total of 3–4 min. This extensive staining removed much of the glycerol and allowed the stain to penetrate the multilayered crystals. Images were recorded at 30,000 magnification with a minimal dose system on a JEOL 1200EX electron microscope on Kodak 4489 film.

Computer analysis

Images were digitized at 20-μm intervals with a flat-bed densitometer (Arndt et al., 1969) connected to a VAX 8600 computer. A well-preserved, crystalline part of each image was selected and isolated from the rest of the image. For images of the (h, k, 0) projection (see Results for assignment of projections), a series of programs developed by Henderson et al. (1986) was used to correct distortions of the crystal lattice. Because these images were relatively large (containing 10,000–15,000 unit cells), small lattice distortions built up into significant displacements across the image and, as a result, diffraction spots in the Fourier transforms were rather diffuse in shape with ill-defined phases. However, by correcting lattice distortions, both the amplitudes and phases of spots were improved dramatically, thereby also increasing the resolution of usable diffraction from ~19 to 15 Å.

After calculating Fourier transforms, the amplitude and phase of each diffraction spot were determined by fitting a sync function to the Fourier data in the vicinity of the spot. Iterative refinement was used to find a common phase origin for the different images. Final amplitudes for each spot were determined by simple averaging of amplitudes from individual images, whereas phases were weighted according to the

signal-to-noise ratio of each spot (Henderson et al., 1986). Projection maps were then calculated without further weighting.

X-Ray diffraction

Hydrated pellets of CaATPase were prepared for x-ray diffraction by pipetting 30–50 μl of crystalline sediment into a 1.0-mm glass x-ray capillary. The capillaries were centrifuged at 1,500 rpm for 10 min at 4°C in a swinging-bucket, bench-top centrifuge. The supernatant was removed and the sample was again centrifuged at 3,200 rpm until a compact pellet was formed (10–20 min). After removing the final supernatant, the capillary was sealed with a flame, care being taken to keep the crystals cold.

X-Ray powder patterns were recorded on two types of cameras, providing different specimen-to-film distances and therefore different resolution ranges. For determination of unit cell parameters, a double mirror camera mounted on a GX 13 rotating anode source with a large specimen-to-film distance of 750 mm was used. The resulting low-angle patterns had a resolution range from ~ 200 to 35 Å and were recorded in 2–6 h with a two-dimensional multiwire detector (Faruqi, 1988). Higher angles were recorded on a toroid camera mounted on a GX 6 rotating anode source with a specimen-to-film distance of 68–75 mm. These patterns were recorded on film, required exposures of 5–12 h and yielded a resolution range of 60–3 Å. The specimen was kept cold (6–8°C) on both cameras by mounting the capillary on a water-cooled copper block.

RESULTS

Crystallization of CaATPase

Crystals were successfully grown from all four preparations of CaATPase (gels shown in Fig. 1). These preparations contained different amounts of lipid (Table 1) and therefore required addition of different amounts of detergent for crystallization. In fact, by adding both detergent and lipid to partially delipidated preparations, a range of crystallization conditions were established. From these experiments, it was apparent that minimum amounts of both lipid and detergent must be present during crystallization.

Preparations of SR1, SR2, and SR3 all required the addition of detergent for crystallization, and the amount of detergent depended on the amount of lipid present. In particular, SR2, which contains a lipid-to-protein ratio of 25:1 (Table 1), crystallized only after adding 25 molar equivalents of detergent. Up to eight times as much detergent could be added without inhibiting crystallization (e.g., detergent-to-lipid-to-protein ratios ranging from 25:25:1 to 200:25:1). However, addition of even more detergent did inhibit crystallization, and addition of too much detergent to preformed crystals dissolved them. Furthermore, exogenous lipid could be added to SR2 as long as equimolar (or more) amounts of detergent were also added to provide a detergent-to-lipid ratio between 1:1 and 8:1. Finally, crystallization of SR1 and SR3 had a similar dependence on detergent. Because these preparations contain more lipid (Table 1), they require correspondingly more detergent for crystallization, but the range of acceptable detergent-to-lipid ratios was comparable.

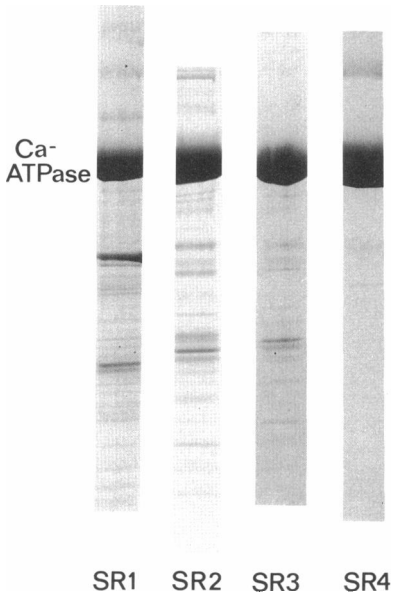

FIGURE 1 Four preparations of CaATPase analyzed by SDS-PAGE. Gels were made with a gradient of acrylamide concentration ranging from 6.5 to 20%, were loaded with 50 μg of protein, and were stained with Coomassie blue. Because the individual lanes shown come from different gels, bands are spaced by different amounts. To show the correspondence between lanes, bands corresponding to CaATPase have been aligned and other equivalent bands are associated by lines running between the lanes. Further details of the preparations, including references, are given in Table 1.

A minimum lipid-to-protein ratio was required for crystallization, which was independent of detergent con-

TABLE 1 Preparations of CaATPase

Preparation	Lipid/protein* molar ratio	
	Before	After‡ delipidation
SR1§	80	10
SR2‖	25	—
SR3¶	110	10
SR4**	—	15

*After digestion of phospholipids with perchloric acid, total phosphorus was determined with the Fiske-Subbarow reagent (McClare, 1971).
‡Delipidation carried out on DEAE column as described in Methods.
§"Native SR" prepared according to Martonosi, 1968.
‖Cholate extraction of SR according to Lüdi and Hasselbach, 1985.
¶Ammonium acetate fractionation of SR according to MacLennan, 1970.
**Affinity column purification according to Coll and Murphy, 1984.

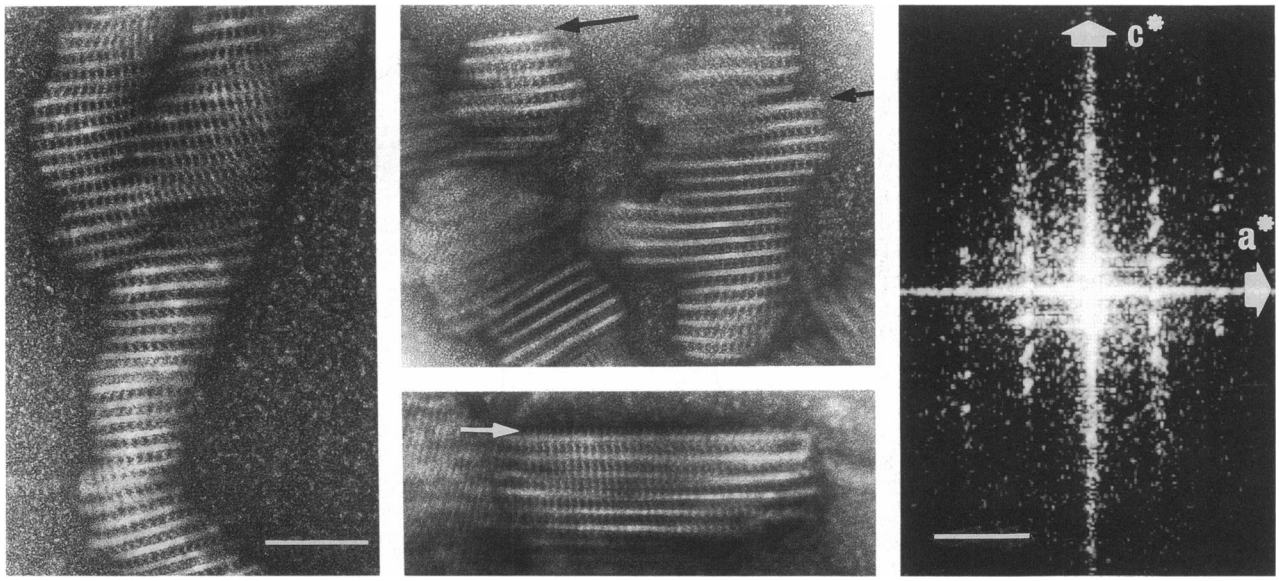

FIGURE 2 The (h, 0, 1) projection. In this view, crystals appear as stacks of stain-excluding layers with projections extending between these layers. The projections can also be seen at the ends of some crystals (*arrows*). A Fourier transform of a selected region is shown on the far right, indicating the orientation of a^* and c^* axes. Odd reflections are not systematically absent along the c^* axis (see also Fig. 3 and Table 4), thereby ruling out the presence of a screw axis along c. Scale bars correspond to 0.1 μm on the micrographs and to 0.01 $Å^{-1}$ on the Fourier transform.

centration within this acceptable range of detergent-to-lipid ratios. In particular, delipidated preparations contained 10–15 mol of lipid per mole of CaATPase (Table 1) and no crystals formed unless the lipid-to-protein ratio exceeded ~25:1. Interestingly, this ratio is approximately that required for full reactivation of delipidated preparations (~30:1 according to Bennett et al., 1980). Because this delipidated protein was eluted from either DEAE or affinity columns, small amounts of detergent were always present, producing detergent-to-lipid-to-protein ratios of ~17:10:1. One could therefore argue that in the absence of added lipid, crystals might have formed at even lower detergent concentrations. Although we cannot eliminate this possibility, it seems unlikely because the detergent-to-lipid ratio (1.7:1) was well within the range found acceptable at slightly higher lipid-to-protein ratios.

Crystal size and morphology varied depending on the exact amount of detergent and lipid present. Minimal amounts of lipid (e.g., detergent-to-lipid-to-protein ratio of 50:25:1) resulted in small (<0.1 μm) crystals that were 1–3 unit cells thick in the c direction (see below for unit cell axes). As lipid was added (e.g., 50:35:1), these small

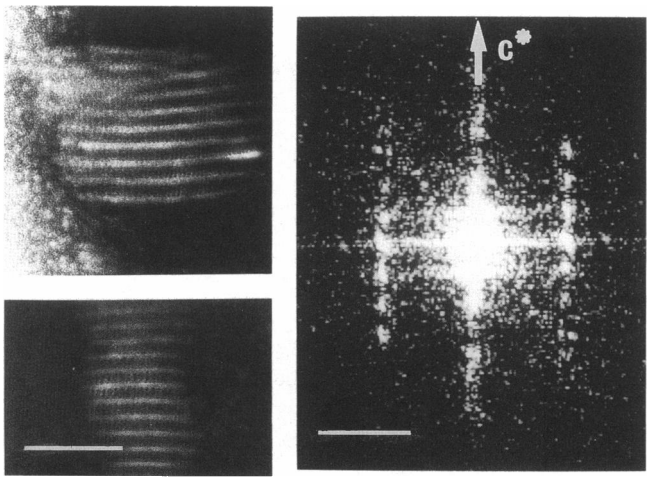

FIGURE 3 The (h, h, 1) projection. This view is much rarer than the (h, 0, 1) projection (Fig. 2) and results in the finer striations seen in the center of each micrograph. The corresponding Fourier transform shows a spacing along c^* similar to the (h, 0, 1) projection (Fig. 2), but a different horizontal spacing. Odd reflections are not absent along the c^* axis (see also Fig. 2 and Table 4), thereby ruling out the presence of a screw axis along c. The scale bars correspond to 0.1 μm and 0.01 $Å^{-1}$.

FIGURE 4 The (h, k, 0) projection. With slightly lower detergent-to-lipid ratios, thin crystals of large diameter are produced, such as that shown here. Micrographs show ribbons of density running parallel to b; the stacking of layers is manifested as steps in density (*arrowheads*) and in a change of pattern at the edges of the crystal. Fourier transforms show a centered lattice and contain reflections to 15 Å resolution. The highest resolution reflections are too weak to be seen by eye, but reflections at resolutions between 20 and 18 Å are visible (*white circles*). Scale bars correspond to 0.1 μm and 0.01 $Å^{-1}$.

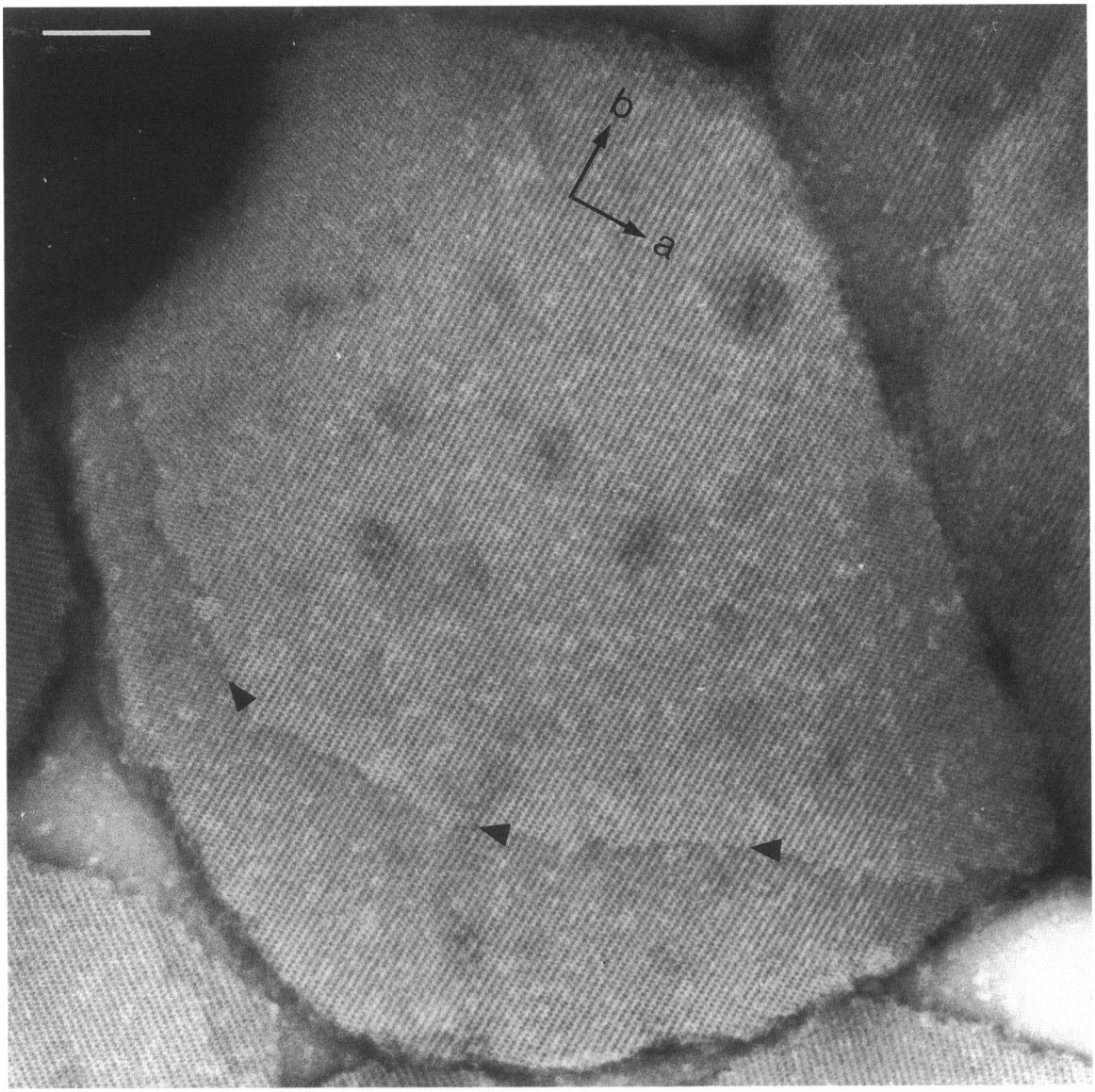
b
a

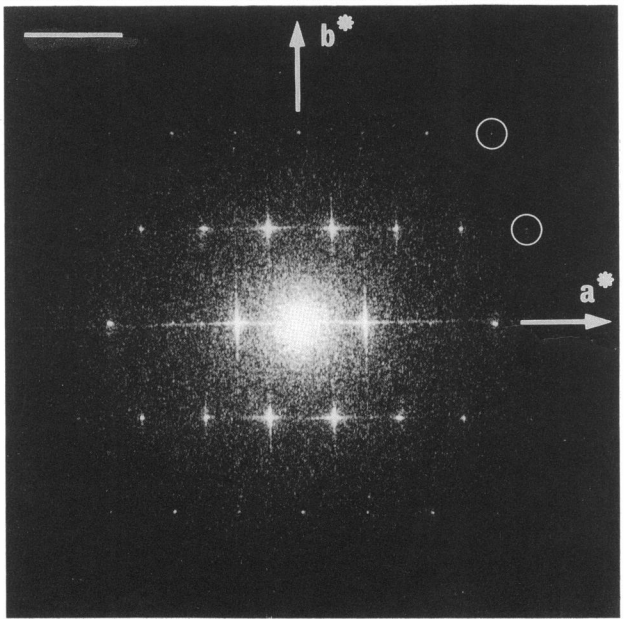
b*
a*

crystals grew predominantly in the c direction, yielding very long (5–10 μm), cylindrical crystals (Figs. 2 and 3). If more lipid was added (e.g., 50:50:1), the crystals grew in the a and b directions producing larger diameter plates that appear to be 5–10 unit cells thick (Fig. 4). If a larger ratio of detergent to protein is used (100:1 or 200:1), a similar pattern of crystal growth was observed, but at correspondingly higher lipid concentrations.

The type of lipid added also affected the crystallization. In particular, unsaturated phosphatidyl cholines (PC), such as dioleoyl PC (Sigma Chemical Co.) or a mixture of PCs isolated from egg yolk (Lipid Products, Redhill, UK), were most effective. Egg yolk phosphatidyl ethanolamine (Sigma Chemical Co.) was also effective, but crystals were considerably smaller and less abundant. No crystals grew from PCs with saturated chains, such as dimyristoyl PC, dipalmitoyl PC, or distearoyl PC (all from Sigma Chemical Co.).

Crystal morphology and symmetry

Three different views of the crystals are seen in the electron microscope and allow assignment of unit cell axes. Two different views are shown in Figs. 2 and 3, which are distinguished by different horizontal periodicities. In both views, the crystals appear as stacks of 40–50 Å thick stain-excluding regions with periodic projections bridging the stain-filled gaps; the direction of stacking has been assigned to the unit cell vector c (see below). An orthogonal view looking along c ((h, k, 0) projection) is shown in Fig. 4. In this view, the crystals appear as plates, which depending on crystallization conditions can be up to 3 μm in diameter. These plates are characterized by regular, stain-excluding ribbons running parallel to b and the stacking along c is often visible as discrete steps in density (arrowheads in Fig. 4). This stacking is also manifested as a change in the pattern of density at the edges of these crystals, indicating that the plates are slightly curved at their edges and provide a view that is no longer exactly along c.

Fourier transforms from the three views are consistent with projections of the monoclinic space group C2. This space group contains a centered lattice in the (h, k, 0) projection, a twofold axis along b, and angles α and γ constrained to be 90°. The centered lattice is clearly seen in the Fourier transform in Fig. 4 with dimensions of a = 151 Å and b = 51 Å with an included angle (γ) of 90.0° (SD = 1.24°, n = 23). Also, the apparent mm symmetry of Fourier amplitudes in this projection is consistent with the presence of the twofold axis and symmetry of Fourier phases indicates that this twofold axis is along b. The c axis corresponds to the vertical periodicity in both Figs. 2 and 3 and has a length of 158 Å. The horizontal periodicity in Fig. 2 is 75 Å, and makes an angle of 89.7° (SD = 3.3, n = 5) with c. This spacing is close to the spacing of the (2, 0, 0) reflection (75.5 Å) in the centered lattice of Fig. 4, suggesting that Fig. 2 represents the (h, 0, l) projection and that 89.7° corresponds to the angle β. The horizontal periodicity in Fig. 3 is 46 Å at an angle of 91.5° (n = 2) to c; comparison of this spacing with that of the (1, 1, 0) reflection (48 Å) in the centered lattice, suggests that Fig. 3 represents the (h, h, l) projection. Thus in terms of C2, the negatively stained unit cell has dimensions of 151 × 51 × 158 Å and an angle β close to 90°.

Higher symmetry space groups can be ruled out by the pattern of amplitudes and phases in Fourier transforms. Because β is so close to 90°, the orthorhombic space groups C222 and $C222_1$ are plausible. In $C222_1$, however, odd reflections are systematically absent along the c^* axis ([0, 0, 1], [0, 0, 3], etc.), which is not observed in Fourier transforms in Figs. 2 and 3 (see also Table 4). Also, C222 contains twofold axes along a, b, and c, whereas C2 contains only one twofold axis along b. As a result, C222 requires strict mm symmetry (amplitudes and phases) in all three principal projections, whereas C2 requires m symmetry in two projections and twofold in the third (i.e., [h, 0, l] projection). Therefore, we examined the symmetry of phases from the (h, k, 0) projection by calculating the average error between individual phases and those expected by either cm ([h, k, 0] = [−h, k, 0] and [h, 0, 0] = 0° or 180°) or cmm (all phases either 0° or 180°) symmetry. We then compared these symmetry-related phase errors with the phase residual from merging individual phases into a single data set and found that the cm-related phase error (7.5°) was somewhat better than the merging phase residual (13.4°), whereas the cmm-related phase error (27.9°) was significantly worse.

X-Ray powder patterns

X-Ray powder patterns were used to measure unit cell spacings in fully hydrated, unstained crystals and to assess the intrinsic order of the crystals. A high-angle pattern is shown in Fig. 5 a and shows diffraction extending to 7.2 Å (marked by a large arrow). The low-angle pattern, shown in Fig. 5 b, can be indexed in C2 with unit cell dimensions of 166 × 58 × 164 Å (Table 2). The orientation of the (0, 0, 1) reflection in the low-angle pattern (arrow in Fig. 5 b) indicates that c is preferentially aligned with the axis of the x-ray capillary. Similar orientation is seen on two higher resolution reflections in the high-angle pattern (small arrows in Fig. 5 a), suggesting that these two reflections lie along the c^* axis. Indeed, their respective spacings (32.3 and 24.2 Å) correspond closely to the (0, 0, 5) and the (0, 0, 7) reflections (32.8 and 23.4 Å), indicating that the stacking along c is ordered to at least 24 Å resolution.

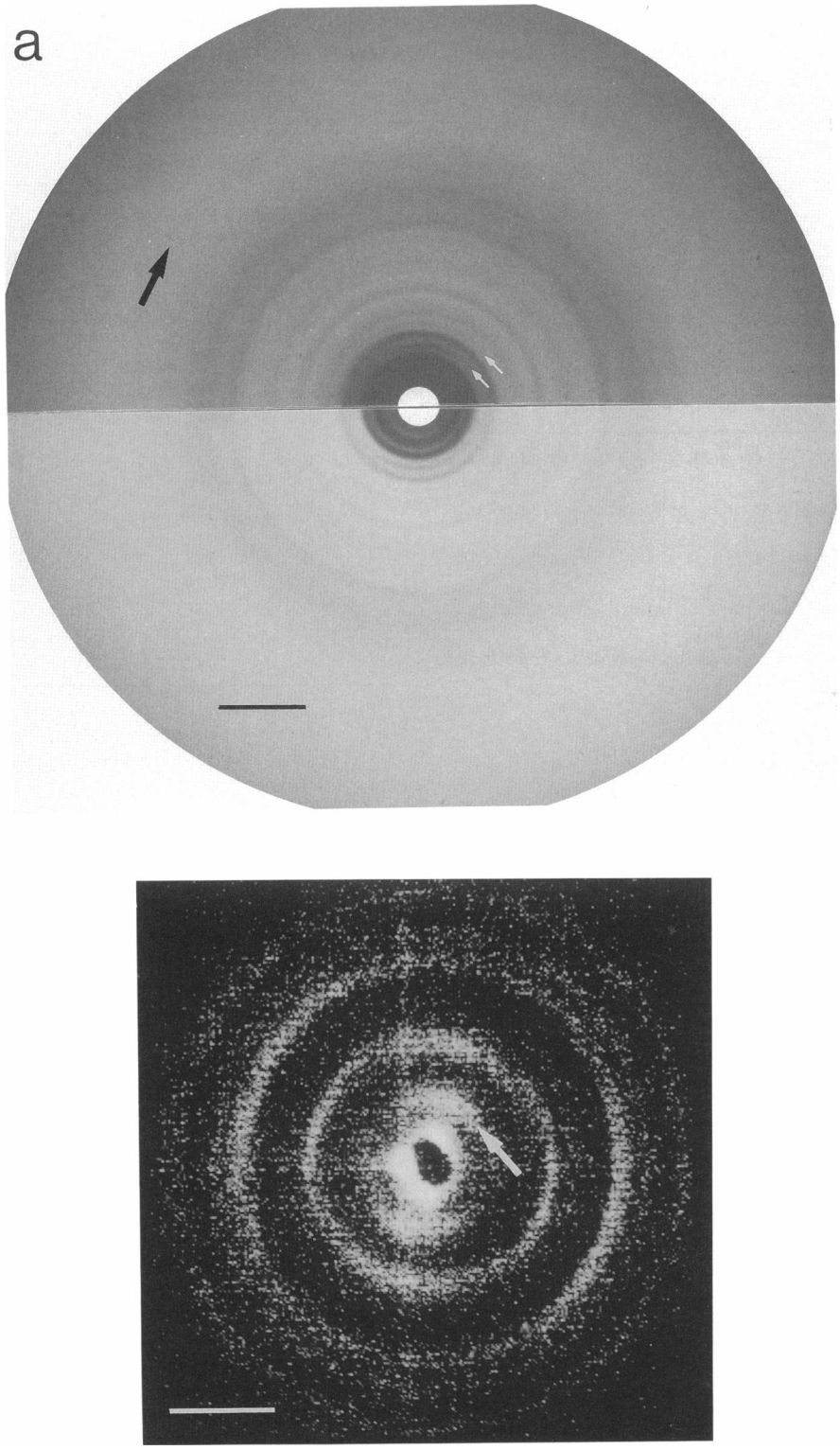

FIGURE 5 X-Ray powder patterns of hydrated, unstained crystals. A high-angle pattern is shown in panel *a* and shows diffraction extending to 7.2 Å resolution (*black arrow*). The upper half of the pattern was printed from the first film in the pack and the lower half from the second film, accounting for the different intensities of the rings. Small white arrows indicate rings at 24.2 and 32.3 Å that are oriented preferentially along the vertical direction (i.e., along the axis of the x-ray capillary). A similar orientation is seen in the innermost ring of the low-angle pattern shown in panel *b*, which was produced on an x-ray detector with the generous help of A. R. Faruqi. This ring is indicated by the large white arrow and is designated as ring 1 in Table 2. The next ring has two components: one oriented parallel to ring 1 (designated 2a in Table 2) and another perpendicular to ring 1 (designated 2b), whereas rings 3 and 4 are composed primarily of components perpendicular to ring 1. Together, these rings can be indexed (see Table 2) with a simple periodicity of 164 Å (components parallel to ring 1) and a centered, two-dimensional lattice of 166 × 58 Å (components perpendicular to ring 1). Thus, components parallel to ring 1 correspond to the stacking of layers (i.e., along *c* axis of crystals) and components perpendicular to ring 1 correspond to the centered, two-dimensional lattice seen in Fig. 4. Small white arrows in panel *a* correspond to higher orders of ring 1 (fifth and seventh orders) and therefore indicate that stacking is ordered to at least 24 Å resolution. Scale bars correspond to 0.04 $Å^{-1}$ in panel *a* and to 0.01 $Å^{-1}$ in panel *b*.

TABLE 2 Indexing of x-ray patterns

Ring on pattern*	Spacing on pattern	Orientation relative to ring 1‡	Index	Expected spacing§
	$Å^{-1}$		*(h, k, l)*	$Å^{-1}$
1	1/163.8	—	(0, 0, 1)	1/164.0
2	1/83.4	a	(0, 0, 2)	1/82.0
		b	(2, 0, 0)	1/83.0
3	1/53.9	a	(0, 0, 3)‖	1/54.7
		b	(1, 1, 0)	1/54.7
4¶	1/41.7	a	(0, 0, 4)‖	1/41.0
		b	(4, 0, 0)	1/41.5
		b	(3, 1, 0)	1/40.0

*The innermost ring in Fig. 5 *b* is designated ring 1 and the outermost is designated ring 4.
‡*a* denotes the same orientation as ring 1 and *b* denotes an orientation perpendicular to ring 1.
§Based on unit cell dimensions of 166 × 58 × 164 Å in the space group C2 with an angle β of 90°.
‖The *a* components of rings 3 and 4 are weak indicating that the (0, 0, 3) and (0, 0, 4) reflections must also be weak.
¶This ring was broader than others, probably reflecting a contribution from both (4, 0, 0) and (3, 1, 0) reflections.

TABLE 3 Amplitudes and phases from (h, k, 0) projection*

Reflection	Amplitude	Phase	R‡	ϕ_{merg}§	ϕ_{sym}‖
(h, k, l)		*degrees*	*%*	*degrees*	*degrees*
2, 0, 0	12550	180	18	2.3	2.6
4, 0, 0	675	0	40	5.1	7.8
6, 0, 0	1134	0	19	3.5	3.5
8, 0, 0	56	0	31	51.3	38.8
10, 0, 0	35	0	28	18.7	21.0
1, 1, 0	5702	−173	8	2.4	1.6
3, 1, 0	2380	28	16	4.0	1.6
5, 1, 0	681	−179	22	5.5	2.8
7, 1, 0	164	175	41	19.8	8.9
9, 1, 0	39	−83	31	55.0	15.9
0, 2, 0	380	161	31	8.3	—
2, 2, 0	198	−59	32	13.9	4.8
4, 2, 0	318	−24	34	5.2	2.6
6, 2, 0	107	72	32	8.6	6.0
8, 2, 0	29	−170	36	32.1	20.1
1, 3, 0	58	42	32	13.5	7.6
3, 3, 0	67	178	32	7.6	5.7
5, 3, 0	20	−81	2	43.3	20.0

*After applying constraints of cm symmetry.
‡R factor for amplitudes defined as $\Sigma (F_i - F_{avg})/F_{avg}$.
§Average phase residual for individual images against merged phases. For whole data set, average phase residual = 13.4°.
‖Average symmetry-related phase error of individual phases. For whole data set, average phase error = 7.5°.

Projection maps

After calculating Fourier transforms and adjusting phase origins, images were averaged together to produce electron density maps of two principal projections. Based on the fidelity of phase information in the (h, k, 0) projection (Table 3 for Fourier data), we concluded that crystals were preserved by uranyl acetate to ~15 Å resolution. The phase residual from merging individual images (no assumed symmetry) increased gradually with resolution, but remained <25° to 15.4 Å resolution (average residual to 14.8 Å was 13.4°). The symmetry-related phase error (cm) was less dependent on resolution and remained <8.5° to 15.4 Å (average error to 14.8 Å was 7.5°). However, the other two projections (h, 0, 1) and (h, h, 1) were susceptible to collapse and shearing, thereby limiting resolution and making the phases of Fourier reflections less reliable. Nevertheless, four images of the (h, 0, 1) projection were merged, thereby generating a phase residual of 30° to 30 Å resolution (Table 4 for Fourier data). When individual phases were compared with those required by twofold symmetry (either 0 or 180°), an average phase error of 26° was found.

The (h, k, 0) projection map is shown at the bottom of Fig. 6 and is characterized by strong density peaks linked into vertical ribbons. The ribbons are in turn linked by weaker density running horizontally. The space group C2 requires four asymmetric units in each unit cell; thus, each of the four strong peaks present in this projection map are related by symmetry and can be associated with an asymmetric unit. Symmetry has not been imposed in this map; nevertheless, cm symmetry is very clearly present.

Two electron density maps of the (h, 0, 1) projection are also shown in Fig. 6, representing data before and after imposing twofold symmetry. The distinct asymmetry in the unsymmetrized map reflects the 26° of symmetry-related phase error present in this data. Nevertheless, the basic features are similar in both maps. A 40-Å-thick stain-excluding layer runs horizontally across the map; the density of the layers is moderately high and relatively unmodulated within the layer. The layers are bridged by density running vertically, which is highly modulated, and which culminates in dominant density peaks 65 Å above and below the center of each stain-excluding layer. Once again, the four dominant peaks are related by symmetry and are each associated with one asymmetric unit. In fact, one set of these peaks can be seen directly in images as bumps protruding from the ends of crystals (arrows in Fig. 2). These bumps extend ~70 Å from the center of the stain-excluding layer and represent the projection of molecules from one layer without superposition of molecules from an adjacent layer. Thus, these bumps establish that peaks in the (h, 0, 1) projection map (Fig. 6) are associated with the closer stain-excluding layer (65 Å away) and not with the further layer (90 Å away).

TABLE 4 Amplitudes and phases from (h, 0, l) projection

Reflection	Amplitude	Phase*	$R^{\ddagger}$	$\phi_{merg}^{\S}$	$\phi_{sym}^{\|}$
(h, k, l)		*degrees*	*%*	*degrees*	*degrees*
0, 0, 1	9576	0	6	61	44
0, 0, 2	1381	0	21	43	33
0, 0, 3	416	0	35	47	52
0, 0, 4	541	180	36	24	24
0, 0, 5	254	0	—	—	—
2, 0, −4	136	0	—	—	—
2, 0, −3	336	0	14	21	28
2, 0, −2	437	180	60	69	34
2, 0, −1	1322	0	25	15	27
2, 0, 0	2380	180	5	9	10
2, 0, 1	1252	0	39	9	9
2, 0, 2	637	0	27	73	28
2, 0, 3	365	180	31	49	44
2, 0, 4	152	0	—	—	—
4, 0, −1	317	180	37	18	26
4, 0, 0	292	0	27	4	18
4, 0, 1	320	180	79	2	2
4, 0, 2	194	0	—	—	—
4, 0, 3	206	0	27	15	16
4, 0, 4	374	180	—	—	—

*To enforce twofold symmetry, phases were constrained to 0 or 180°.
‡R for amplitudes defined as $\Sigma (F_i - F_{avg})/F_{avg}$.
§Average phase residual for individual images against merged phases. For whole data set, average phase residual = 30°.
‖Average symmetry-related phase error of individual phases. For whole data set, average phase error = 26°.

DISCUSSION

Microcrystals of CaATPase have been studied and appear to be three-dimensional crystals that are well ordered and highly suitable for electron microscopy. Electron micrographs of negatively stained crystals show stacks of 40-Å-thick stain-excluding layers with periodic projections holding these layers apart (Figs. 2 and 3); an orthogonal view shows a well-ordered, centered lattice within the plane of each layer (Fig. 4). These micrographs verify that the crystals belong to the first of two types of membrane proteins, called type I (Michel, 1983). Few examples of type I crystals exist, and those that have been thoroughly studied have disordered stacking (Kühlbrandt, 1988*a*; Henderson and Shotton, 1980). It is therefore noteworthy that x-ray powder patterns from these CaATPase crystals not only show diffraction at 7.2 Å resolution, but also show that stacking is ordered. Furthermore, their thin, platelike morphology is well suited for electron microscopy, which could, in an unstained preparation, potentially provide information at 7 Å resolution. In the meantime, we will use micrographs of negatively stained crystals to describe crystal symmetry and molecular packing.

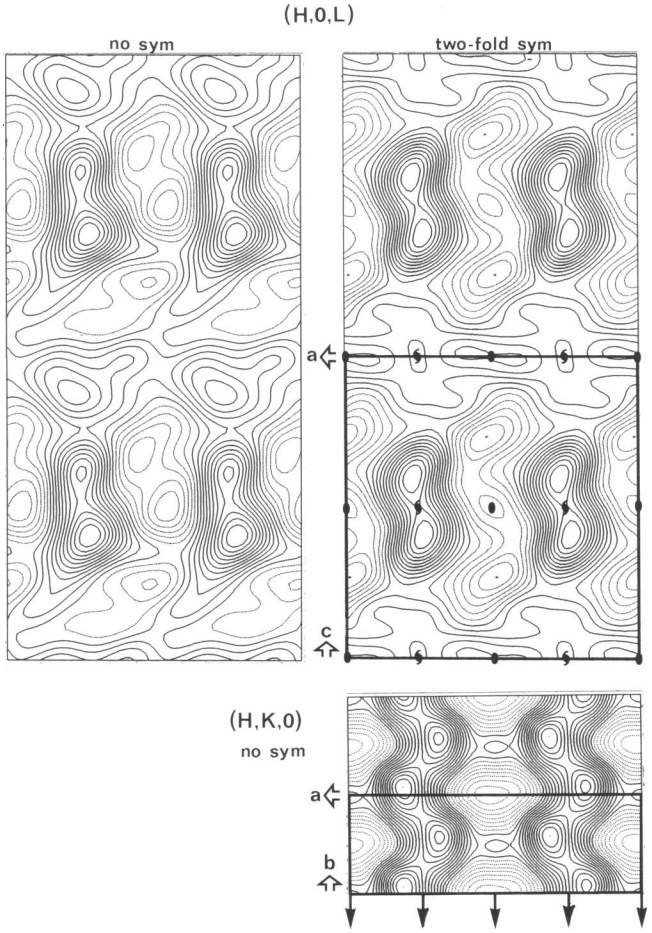

FIGURE 6 Density maps of (h, k, 0) and (h, 0, l) projections. Solid contours represent stain-excluding regions, whereas dotted contours represent regions of stain accumulation. A single unit cell is outlined for each projection and the locations of symmetry axes are marked. The (h, 0, l) projection maps are shown both before and after imposing twofold symmetry, but no symmetry has been imposed in the (h, 0, l) projection map.

Composition of stain-excluding layers

The stain-excluding layers visible in the (h, 0, l) and (h, h, l) projections (Figs. 2 and 3) suggest the presence of a planar hydrophobic region that resembles a lipid bilayer. This conclusion, which was also reached by Taylor et al. (1988), is based on the relatively uniform exclusion of stain from this 40-Å-thick layer and on the observed requirement of lipid for crystallization (~25 mol lipid/mol protein). However, these stain-excluding layers cannot be ordinary membranes for two reasons. First, detergent is present in concentrations large enough to solubilize all of the lipid required for crystallization, and second, unlike pure lipid membranes, the layers in these

crystals are disk-shaped and the disks have edges that appear to be open to aqueous solvent.

This suggests that detergent may have two distinct roles in the crystal. The first is to shield the hydrophobic tails along the edges of these disks by forming a micellar annulus of detergent around these edges. The second role is as a component of the hydrophobic layer within each unit cell, perhaps satisfying specific structural requirements of CaATPase. Although we have no direct evidence for either role, the presence of detergent at the edges may control the size of crystals, similar to the role of deoxycholate in the mixed micelles that it forms with lipid (Müller, 1981). Specifically, we observed that large detergent-to-lipid ratios produce small-diameter crystals and that the diameter increases as lipid is added. This is similar to the size dependence of these mixed micelles, which consist of a disk-shaped, mixed bilayer of lipid and deoxycholate surrounded by an annulus of deoxycholate molecules. Due to the geometry of this structure, the perimeter-to-area ratio will reflect the detergent-to-lipid ratio and an addition of lipid is accommodated by simply making disks with larger diameters (Müller, 1981).

Crystal symmetry and molecular packing

The symmetry of our crystals is consistent with previous observations except that we observe order in the third dimension. In particular, Taylor et al. (1988) speculated that the symmetry of each layer was consistent with the two-sided plane group c12 but that the stacking of layers was probably disordered. Our measurements of symmetry-related phase errors in the (h, k, 0) projection confirms this c12 symmetry, but ordered stacking is clearly seen both in electron micrographs of the (h, 0, 1) and (h, h, 1) projections (Figs. 2 and 3) and in x-ray powder patterns (Fig. 5). We therefore conclude that the crystals belong to the three-dimensional space group C2.

Even though C2 is a monoclinic space group, the angle β appears to be close to 90°, as expected of orthorhombic space groups. Measurements from (h, 0, 1) projections directly show β to be close to 90°, though the susceptibility of these long, narrow crystals to shearing (see Fig. 2) means that this measurement is somewhat unreliable. However, the larger, platelike crystals provide a more stable morphology, and the high frequency of (h, k, 0) projections from these crystals confirms that β is close to 90°, as follows. These plates lie flat on the surface of the carbon-coated em grid (Fig. 4) and therefore the plane of the hydrophobic layer, which is coplanar with the *a-b* plane of the crystals, must be normal to the incident electron beam (the specimen holder was fixed at 0° tilt). Because the (h, k, 0) projection results from a view directly down the *c* axis, *c* must also be normal to the *a-b* plane. Otherwise, the specimen would have to be tilted to obtain the (h, k, 0) projection, which is easily recognized due to its cm symmetry.

The existence of this planar hydrophobic region can also be used to deduce the presence of four CaATPase molecules in each unit cell. In the space group C2, the unit cell contains four asymmetric units, generating possibilities for 4, 8, 12, etc. molecules per unit cell, corresponding to 1, 2, 3, etc. molecules per asymmetric unit. As previously argued by Taylor et al. (1988), the intramembranous portion of CaATPase must pack together with lipid and possibly with detergent into this hydrophobic layer. Because the intramembranous portion of one CaATPase molecule has been shown to occupy between 1,200 (Taylor et al., 1986*b*) and 2,200 Å^2 (Herbette et al., 1985), the area available per unit cell (9,600 Å^2) is large enough for four, but not for eight CaATPase molecules. Given four molecules, the unit cell would provide 3.6 Å^3/D protein (Matthews, 1968) and proportionately less per dalton of protein and lipid; stated in another way, these four molecules would occupy ~35% of the unit cell volume, which leaves ample room for lipid and detergent.

A scheme for packing these four CaATPase molecules into the unit cell is depicted in Fig. 7. This scheme relies on a comparison of density in the two projection maps with low-resolution structures of CaATPase, previously determined from two-dimensional crystals in SR membranes (Castellani et al., 1985; Dux et al., 1985; Taylor et al., 1986*a*). The extramembranous domain of CaATPase is almost entirely on one side of the membrane and extends to ~60 Å above the membrane surface. This domain consists of a pear-shaped head (65 × 40 × 50 Å) centered ~35 Å above the cytoplasmic surface of the membrane and connected to it by a 28-Å-diameter stalk. The pear shape is conferred by a smaller lobe, which protrudes away from the stalk ~30 Å from the membrane surface. In negative stain, this extramembranous domain, and particularly the head, is the dominant feature of electron density maps because intramembranous domains are hidden within the stain-excluding lipid bilayer. Thus, the "bumps" protruding from the edges of (h, 0, 1) projections (arrows in Fig. 2) resemble the heads of CaATPase molecules that are inserted into the top-most hydrophobic layer. In the corresponding projection map (Fig. 6), the large distance between adjacent hydrophobic layers (158 Å) results in only a few angstroms of overlap between molecules protruding from adjacent layers. We have therefore assigned the highest density peak, which is ~40 Å from the surface of the hydrophobic layer, to the head of CaATPase. This peak is connected to the hydrophobic layer by a 30-Å-wide band of lower density, which we therefore assign to the stalk.

Unfortunately, the (h, k, 0) projection contains significant overlap between molecules above and below the

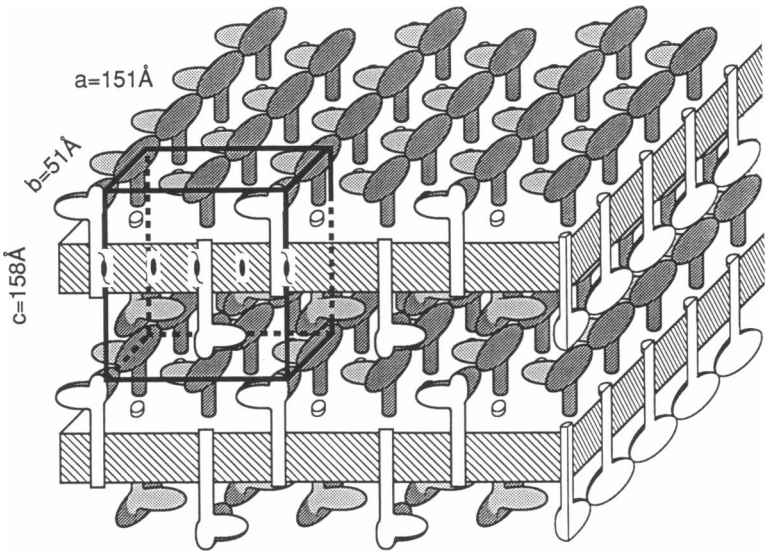

FIGURE 7 Packing diagram for CaATPase crystals. A CaATPase molecule is depicted as two ellipsoids on a narrow cylinder placed asymmetrically into the planar, hydrophobic layer. This rough shape is derived from previous three-dimensional reconstructions from two-dimensional crystals (Castellani et al., 1985; Taylor et al., 1986*a*). Molecules at the front and on the right margins have been sectioned to reveal the portion crossing the hydrophobic layer, which in reality is slightly larger than depicted here. A unit cell has been drawn on the left, though for clarity the origin is displaced vertically relative to Fig. 6; the unit cell dimensions are those deduced from hydrated specimens. Proposed molecular contacts occur along the axis of stacking (*c*), between the tops of CaATPase heads, and along the axis of ribbons (*b*), between the sides of CaATPase heads. The contact between ribbons (along *a*) has not been observed and may therefore be close to or within the hydrophobic layer.

hydrophobic layers, which makes interpretation of the map (Fig. 6) more difficult. However, with further reference to three-dimensional structures from two-dimensional crystals (Castellani et al., 1985; Taylor et al., 1986*a*), the bulk of the extramembranous domain appears to be located in a 25–30-Å-diameter column lying perpendicular to the membrane surface and centered on the stalk. Thus, we believe that the strong peaks in our (h, k, 0) map (Fig. 6), which are separated by 26 Å along *b* and by 15 Å along *a*, correspond to this column of density. The 15 Å displacement along *a* (shown in Fig. 7) is not clear in the (h, 0, 1) projection; this may be either because of the specific way in which density is summed in this projection or possibly because of phase error in the corresponding Fourier data.

This provides the basic arrangement of molecules in the hydrophobic layer, but the rotational orientation of the molecule about an axis parallel to *c* remains less certain. Two types of two-dimensional crystals from SR (so-called E1 and E2 crystals) are also composed of ribbons and therefore offer two distinct possibilities. In E2 crystals, the low-density lobe is oriented parallel to the axis of the ribbons (Fig. 8 *a*, from Taylor et al., 1986*a*), whereas this lobe is 90° to the ribbon axis in E1 crystals (Fig. 8 *b*, from Dux et al., 1985). It is plausible that the contacts along the ribbons in E1 crystals are preserved in our three-dimensional crystals, because the repeats are similar (50.4–54.4 Å in E1 crystals compared with 51 Å in three-dimensional crystals) and both crystallization conditions contain high concentrations of calcium. Therefore, Fig. 8 attempts to relate the packing in both E1 and E2 crystals to that in three-dimensional crystals. Because in SR, CaATPase protrudes from only one side of the membrane, an additional set of molecules must be added, representing symmetry-related molecules protruding from the other side of the hydrophobic layer. Also, the spacing between ribbons has been artificially adjusted to correspond to the spacing observed in three-dimensional crystals. Thus, Fig. 8 *d* shows that E1 crystal packing not only provides a similar repeat along the ribbon axis, but also suggests that the weak density running along *a* in (h, k, 0) projection maps can be accounted for by the small cytoplasmic lobe. Therefore, we have tentatively adopted this particular rotational orientation for our packing model (Fig. 7), and will seek, in the future, to confirm this orientation with three-dimensional data.

Intermolecular contacts

Contacts between molecules can be deduced from this packing model (Fig. 7) with reference to the two projection maps (Fig. 6). A major contact must run along *c* and thereby cause the layers to stack. As described, the molecules are expected to overlap only slightly along *c*, so

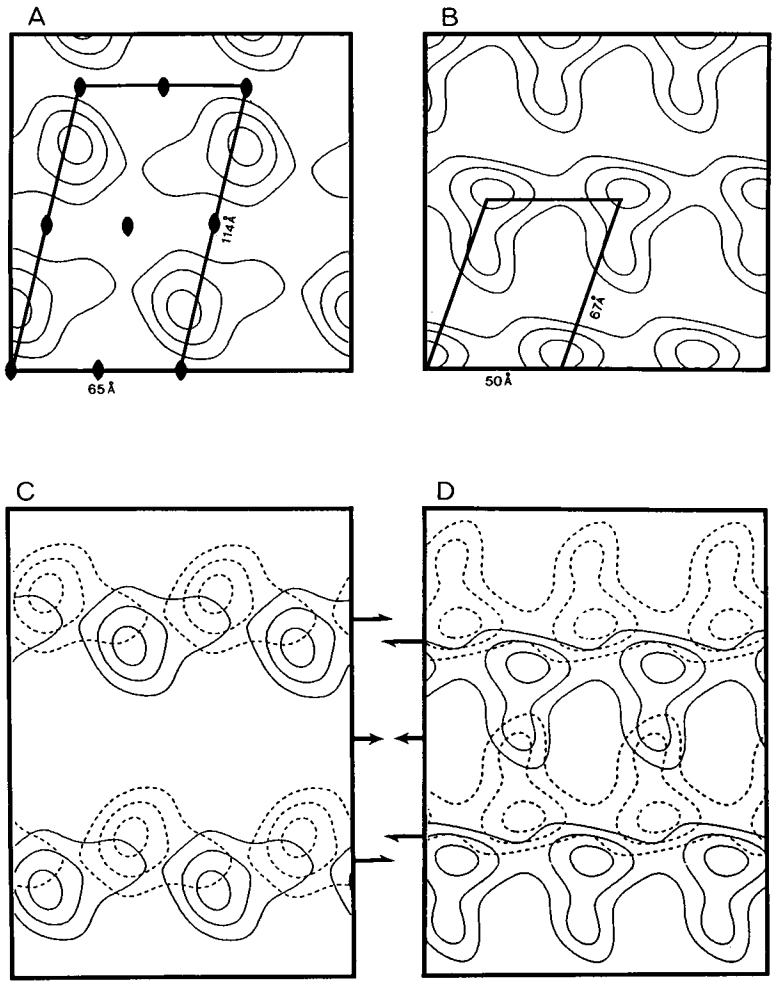

FIGURE 8 Relationship between crystal packing in these three-dimensional crystals and that in two-dimensional crystals from SR. Projection maps looking normal to the membrane plane are shown in *a* for vanadate-induced E_2 crystals, and in *b* for praseodymium-induced E_1 crystals. Because these crystals occur in native SR, molecules project from only one side of the membrane (cytoplasmic side). Simulated projection maps of three-dimensional crystals (*c* and *d*) have been derived from their respective counterparts (*a* and *b*) by isolating a single, horizontal ribbon and applying the appropriate in-plane, twofold symmetry. The dotted contours represent these symmetry-related molecules, which project from the opposite side of the membranous layer (corresponding to the luminal side of SR). The distance between ribbons has been adjusted in proportion to the repeat along the ribbons, accounting for the larger spacings in panel *c*. Based on these comparisons, the packing depicted in panel *d* seems the most likely, both because the 50-Å spacing is quite similar to that observed in three-dimensional crystals and because the weak density running between ribbons is accounted for (see [h, k, 0] projection in Fig. 6). The data used to construct *a* was taken from Taylor et al. (1984), whereas that in *b* was kindly supplied by Ken Taylor (also see Dux et al., 1985).

this contact must be between the top-most surfaces of molecules from adjacent layers. Accordingly, the (h, 0, l) projection map shows strong vertical connection along *c*, which must result in part from this crystalline contact and in part from fortuitous overlap of density. In contrast, no positive density extends horizontally along *a* outside of the hydrophobic layer, and in the (h, k, 0) projection map, only weak density connects ribbons along *a*. As described above, this weak density may be accounted for by the small cytoplasmic lobe, which cannot provide the contact along *a* due to its position ~30 Å from the surface of opposing hydrophobic layers (see Fig. 7). It seems likely, therefore, that this contact along *a*, which is responsible for holding ribbons together, is either close to or within the hydrophobic layer. The contact along the axis of these ribbons (i.e., along *b*) is obscured by overlapping density in our projection maps. However, as set forth in Fig. 8, this contact may be similar to that in two-dimensional, E1 crystals. This conclusion is strengthened by our observation of single-layered crystals in some of our crystallization conditions (data not shown). This observation suggests that connections along the ribbons, as well as those

between ribbons, can be made among molecules in a single layer and do not need to be mediated by molecules from adjacent layers. The stacking of layers, however, may serve to stabilize the two-dimensional lattice within each layer.

Conclusion

The negatively stained crystals of CaATPase appear well ordered in three dimensions and have been useful in characterizing crystal morphology (type I), symmetry (space group C2), and molecular packing (Fig. 7). X-Ray diffraction of unstained crystals demonstrates that they are ordered to 7 Å resolution, but diffraction studies of single crystals are not possible due to their microscopic size. Nevertheless, electron microscopy could provide this resolution if an unstained preparation were developed, either by rapid freezing (Taylor and Glaeser, 1976) or by embedding the crystals in glucose (Unwin and Henderson, 1975). Such preparations do not suffer from the limitations inherent to negative stain, namely low resolution and visualization of the stain envelope rather than of the protein itself. Therefore, a three-dimensional reconstruction of an unstained preparation of 7 Å resolution could reveal the arrangement of alpha-helices in the protein. There may be technical difficulties in electron microscopy of so thick an object, but attempts are justified by the possibility of interpreting the amino acid sequence of CaATPase, and several related ion pumps, on a truly physical basis.

We gratefully acknowledge Richard Henderson, without whose expertise these studies could not have been done. We also thank Jade Li and A. R. Faruqi for their assistance with x-ray experiments, Nick Wrigley for the use of his microscope, Claudio Villa for many hours of photography, Brian Pashley for drafting the packing diagram, and Chikashi Toyoshima for his critical reading of the manuscript. Finally, we thank Ken Taylor for his critisms regarding our packing model and for providing the data used to construct Fig. 8.

D. L. Stokes was supported by a fellowship from the Muscular Dystrophy Association.

Received for publication 1 May 1989 and in final form 14 August 1989.

REFERENCES

Arndt, U. W., J. Barrington-Leigh, J. F. W. Mallet, and K. E. Twinn. 1969. A mechanical microdensitometer. *J. Phys. E Sci. Instrum.* 2:385–387.

Bennett, J. P., K. A. McGill, and G. B. Warren. 1980. The role of lipids in the functioning of a membrane protein: the sarcoplasmic reticulum calcium pump. *In* Current Topics in Membranes and Transport: Carriers and Membrane Transport Proteins. F. Bronner and A. Kleinzeller, editors. Academic Press Inc., New York. 127–164.

Castellani, C., P. M. D. Hardwicke, and P. Vibert. 1985. Dimer ribbons in the three-dimensional structure of sarcoplasmic reticulum. *J. Mol. Biol.* 185:579–594.

Clarke, D. M., T. W. Loo, G. Inesi, and D. H. MacLennan. 1989. Location of high affinity Ca^{2+}-binding sites within the predicted transmembrane domain of the sarcoplasmic reticulum Ca^{2+}-ATPase. *Nature (Lond.).* 339:476–478.

Coll, R. J., and A. J. Murphy. 1984. Purification of the CaATPase of sarcoplasmic reticulum by affinity chromatography. *J. Biol. Chem.* 259:14249–14254.

Deisenhofer, J., O. Epp, K. Miki, R. Huber, and H. Michel. 1985. Structure of the protein subunits in the photosynthetic reaction center of *Rhodopseudomonas viridis* at 3Å resolution. *Nature (Lond.).* 381:618–624.

Dux, L., K. A. Taylor, H. P. Ting-Beall, and A. Martonosi. 1985. Crystallization of the Ca^{2+}-ATPase of sarcoplasmic reticulum by calcium and lanthanide ions. *J. Biol. Chem.* 260:11730–11743.

Dux, L., S. Pikula, N. Mullner, and A. Martonosi. 1987. Crystallization of Ca^{2+}-ATPase in detergent-solubilized sarcoplasmic reticulum. *J. Biol. Chem.* 262:6439–6442.

Faruqi, A. R. 1988. Development and application of multiwire detectors in biological x-ray studies. *Nucl. Instrum. Meth. Phys. Res.* A273:754–763.

Garavito, R. M., J. Jenkins, J. N. Jansonius, R. Karlsson, and J. P. Rosenbusch. 1983. X-Ray diffraction analysis of marix porin, an integral membrane protein from *Escherichia coli* outer membranes. *J. Mol. Biol.* 164:313–327.

Green, N. M. 1975. The role of lipid in stabilisation and activation of the Ca^{++} transporting ATPase of sarcoplasmic reticulum. *In* Calcium Transport in Contraction and Secretion. E. Carafoli, F. Clementi, W. Drabikowski, and A. Margreth, editors. North-Holland Publishing Co., Amsterdam. 339–348.

Henderson, R., and D. Shotton. 1980. Crystallization of purple membrane in three dimensions. *J. Mol. Biol.* 139:99–109.

Henderson, R., J. M. Baldwin, K. H. Downing, J. Lepault, and F. Zemlin. 1986. Structure of purple membrane from *Halobacterium halobium:* recording, measurement and evaluation of electron micrographs at 3.5 Å resolution. *Ultramicroscopy.* 19:147–178.

Herbette, L., P. DeFoor, S. Fleischer, D. Pascolini, A. Scarpa, and J. K. Blasie. 1985. The separate profile structures of the functional calcium pump protein and the phospholipid bilayer within isolated sarcoplasmic reticulum membranes determined by x-ray and neutron diffraction. *Biochim. Biophys. Acta.* 817:103–122.

Inesi, G. 1985. Mechanism of calcium transport. *Annu. Rev. Physiol.* 47:573–601.

Kühlbrandt, W. 1988*a*. The structure of light-harvesting chlorophyll a/b protein complex from plant photosynthetic membranes at 7Å resolution in projection. *J. Mol. Biol.* 202:849–864.

Kühlbrandt, W., 1988*b*. Three-dimensional crystallization of membrane proteins. *Q. Rev. Biophys.* 21:429–477.

Lüdi, H., and W. Hasselbach. 1985. Preparation of a highly concentrated, completely monomeric, active sarcoplasmic reticulum Ca^{++}-ATPase. *Biochim. Biophys. Acta.* 821:137–141.

MacLennan, D. H. 1970. Purification and properties of an adenosine triphosphatase from sarcoplasmic reticulum. *J. Biol. Chem.* 245:4508–4518.

Martonosi, A. 1968. Sarcoplasmic reticulum. IV. Solubilization of microsomal adenosine triphosphatase. *J. Biol. Chem.* 243:71–81.

Martonosi, A., K. A. Taylor, S. Varga, and H. Ping Ting-Beall. 1987. The molecular structure of sarcoplasmic reticulum. *In* Electron

Microscopy of Proteins: Membranous Structures. J. R. Harris and R. W. Horne, editors. Academic Press Inc., London. 255–376.

Maruyama, K., and D. H. MacLennan. 1988. Mutation of aspartic acid-351, lysine-352, and lysine-515 alters the Ca^{2+} transport activity of the Ca^{2+}-ATPase expressed on COS-1 cells. *Proc. Natl. Acad. Sci. USA.* 85:3314–3318.

Matthews, B. W. 1968. Solvent content of protein crystals. *J. Mol. Biol.* 33:491–497.

McClare, C. W. 1971. An accurate and convenient organic phosphorus assay. *Anal. Biochem.* 39:527–530.

Michel, H. 1983. Crystallization of membrane proteins. *Trends Biochem. Sci.* 8:56–59.

Müller, K. 1981. Structural dimorphism of bile salt/lecithin mixed micelles. A possible regulatory mechanism for cholesterol solubility in bile? X-Ray structure analysis. *Biochemistry.* 20:404–414.

Taylor, K. A., and R. Glaeser. 1976. Electron microscopy of frozen hydrated biological specimens. *J. Ultrastruct. Res.* 55:448–456.

Taylor, K., L. Dux, and A. Martonosi. 1984. Structure of the vanadate-induced crystals of sarcoplasmic reticulum Ca^{2+}-ATPase. *J. Mol. Biol.* 174:193–204.

Taylor, K. A., L. Dux, and A. Martonosi, 1986*a*. Three-dimensional reconstruction of negatively stained crystals of the Ca^{++}-ATPase from muscle sarcoplasmic reticulum. *J. Mol. Biol.* 187:417–427.

Taylor, K. A., M.-H. Ho, and A. Martonosi. 1986*b*. Image analysis of the Ca^{2+}-ATPase from sarcoplasmic reticulum. *Ann. NY Acad. Sci.* 483:31–43.

Taylor, K. A., N. Mullner, S. Pikula, L. Dux, C. Peracchia, S. Varga, and A. Martonosi. 1988. Electron microscope observations on Ca^{2+}-ATPase microcrystals in detergent-solubilized sarcoplasmic reticulum. *J. Biol. Chem.* 263:5287–5294.

Unwin, P. N. T., and R. Henderson. 1975. Molecular structure determination by electron microscopy of unstained crystalline specimens. *J. Mol. Biol.* 94:425–440.